Journal of Materials Chemistry A

Accepted Manuscript

ROYAL SOCIETY OF CHEMISTRY

www.rsc.org/materialsA

Journal Name

ARTICLE

Robust α-Fe_2O_3 nanorod arrays with optimized interstices as high-performance 3D anodes for high-rate lithium ion batteries†

Received 00th January 20xx,

Accepted 00th January 20xx

DOI: 10.1039/x0xx00000x

www.rsc.org/

Shuai Chen,‡ Yuelong Xin,‡ Yiyang Zhou, Feng Zhang, Yurong Ma, Henghui Zhou,* and Limin Qi*

Self-supported α-Fe_2O_3 nanorod arrays consisting of mesocrystalline nanorod bundles with tunable interstices were prepared by solution-phase growth coupled with chemical etching. The existence of acetic acid and sulfate ions in the hydrothermal system promoted the direct growth of α-Fe_2O_3 nanorod bundles with a mesocrystalline structure on Ti substrate. The robust α-Fe_2O_3 nanorod arrays with optimized interstices are able to offer reduced lengths for electronic transport and ionic diffusion, and enough spaces to accommodate lithiation-induced volume expansion, leading to novel three-dimensional (3D) anodes with significantly improved rate capability and cyclability. When used as a binder-free anode for lithium ion batteries (LIBs), the α-Fe_2O_3 nanorod arrays retained a reversible capacity of 801 mAh g^{-1} after 500 cycles at 5 C (namely, 5 A g^{-1}), and achieved practically valuable capacities of 499 mAh g^{-1} and 350 mAh g^{-1} at high rates of 20 C and 30 C, respectively. Furthermore, a flexible LIB full battery with high capacity and fast charging capability was assembled using the α-Fe_2O_3 nanorod arrays as the anode, demonstrating their potential applications in flexible electronics.

Introduction

Rechargeable lithium ion batteries (LIBs) have been widely considered to be one promising energy storage technology for portable devices, flexible electronics, electric vehicles, and stationary energy storage owing to the advantages of high energy density, long cycle life, and environmental benignity.[1-3] To meet the increasing demands of new energy sources with less charging time and higher output power, advanced LIBs with high energy density, high power density and long lifespan are highly required. Accordingly, great efforts have been devoted to developing new electrode materials with superior architectures to improve rate capability and cycling stability.[4-6] Meanwhile, there is immense interest in establishing greener and more sustainable LIBs by taking into account element abundance, toxicity, and synthetic methods.[7] In this regard, α-Fe_2O_3 is a promising candidate for high-performance LIB anodes because of its high theoretical capacity (~1000 mAh g^{-1}), non-toxicity, high abundance, high corrosion resistance, and low processing cost.[8] However, α-Fe_2O_3 anodes usually suffer from poor cyclability caused by the drastic volume expansion during lithiation and the performance degradation at high current densities associated with the low conductivity. Generally, improved rate performance and prolonged cycling stability can be achieved through the design and synthesis of nanostructured α-Fe_2O_3 materials possessing enhanced electrochemical activity, reduced ionic/electronic diffusion length, and capability to buffer the volume strain as well as the fabrication of hybrid nanostructures of α-Fe_2O_3 and conductive materials.[8] For example, a variety of α-Fe_2O_3 nanostructures with improved electrode performance, such as porous particles,[9,10] hollow structures,[11-16] mesocrystals,[17,18] nanotubes,[19] nanomembranes,[20] and nanoarrays,[21-23] have been reported together with α-Fe_2O_3-based nanohybrids with graphene,[24,25] carbon nanotubes (CNTs)[26] and conductive polymer.[27,28] Nevertheless, it remains a challenge to fabricate high-performance α-Fe_2O_3 nanostructures with optimized architectures for high-rate LIBs at low processing cost.

Recently, the electrodes based on three-dimensional (3D) self-supported nanostructured metal oxides have become increasingly important for the miniaturization of energy storage systems.[29] In particular, ordered arrays of one-dimensional (1D)[28,30-33] and two-dimensional (2D)[34] metal oxide nanostructures grown directly on current collecting substrates have been demonstrated to be high-performance 3D anodes for LIBs. These self-supported 3D electrodes hold many inherent advantages for high-rate LIBs including high surface area, reduced lengths for electronic transport and ionic diffusion, tunable spaces for accommodating volume expansion, and adherence of the active material to the current collector. Furthermore, the self-supported nanoarrays are promising candidates as binder-free electrodes in flexible LIBs, which show potential applications in soft electronic products, roll-up displays, and wearable devices.[3,35] Notably, self-supported arrays of α-Fe_2O_3 nanorods,[21] nanotubes,[22] and nanowalls[23] grown on conductive substrates have shown

Beijing National Laboratory for Molecular Sciences, State Key Laboratory for Structural Chemistry of Unstable and Stable Species, College of Chemistry, Peking University, Beijing 100871, China. E-mail: hhzhou@pku.edu.cn; liminqi@pku.edu.cn

† Electronic Supplementary Information (ESI) available: [Additional optical photographs and SEM images]. See DOI: 10.1039/x0xx00000x

‡ These authors contributed equally to the work.

enhanced rate performance for LIBs. However, these α-Fe_2O_3 nanoarrays were usually fabricated through conversion form $Fe(OH)_3$ nanoarrays and hence exhibited poor cycling performance at high current densities owing to the unfavorable structural stability. On the other hand, mesocrystals, which are crystallographically oriented nanoparticle superstructures characterized by high crystallinity, high porosity, and oriented subunit alignment,[36] have strong potential as electrode materials for LIBs since they would possess the structural stability of microsized electrodes while exploiting the beneficial properties associated with nanosized electrodes.[37,38] Nevertheless, it remains a challenge to realize the direct growth of robust, mesocrystalline α-Fe_2O_3 nanoarrays on conductive substrates. Therefore, it would be highly desirable to develop new synthetic strategies towards robust, self-supported α-Fe_2O_3 nanoarrays with optimal architectures for high-rate LIBs with superior cycling stability.

Herein, we report a novel synthesis of robust, mesocrystalline α-Fe_2O_3 nanorod arrays with optimized interstices by hydrothermal growth coupled with structural optimization through chemical etching. As shown in Fig. 1a, dense arrays of hierarchical α-Fe_2O_3 nanorod bundles were directly grown on Ti substrate in acetic acid (HAc) solutions assisted by sulfate ions. Then, the interstices between nanorods were readily adjusted by etching with oxalic acid solutions, resulting in appropriate void spaces to buffer the lithiation-induced volume expansion and benefit the infiltration of electrolyte. Owing to the tight adherence of the nanoarrays to the Ti substrate as well as the optimized interstices between nanorods, the self-supported α-Fe_2O_3 nanorod arrays are able to withstand many charge-discharge cycles and maintain good structural integration, whereas the pristine α-Fe_2O_3 nanoarrays with limited spaces undergo pulverization gradually upon multiple cycles (Fig. 1b). The optimized α-Fe_2O_3 nanorod arrays exhibited excellent cyclability (retained a reversible capacity of 801 mAh g^{-1} after 500 cycles at 5 C, 1 C = 1000 mA g^{-1}) and high rate capability when used as a binder-free anode for LIBs. Furthermore, a flexible LIB full cell with high capacity and fast-charging capability was assembled by using the α-Fe_2O_3 nanorod arrays as a flexible anode to demonstrate their potential applications in flexible electronics.

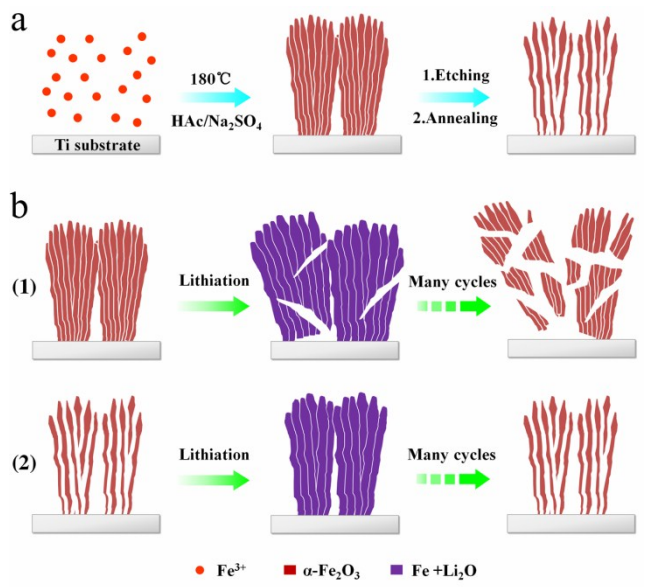

Fig. 1 Schematic illustration of (a) the formation of α-Fe_2O_3 nanorod arrays with optimized interstices and (b) the structure evolution of pristine (1) and optimized (2) α-Fe_2O_3 nanorod arrays during cycling processes.

Experimental section

Materials and synthesis

Ti foils (0.05 mm in thickness, 99.6%, Alfa-Aesar) were cleaned by sonication in acetone, ethanol, deionized (DI) water, and finally dried in air. α-Fe_2O_3 nanorod arrays were grown directly on Ti foil by a facile hydrothermal method. In a typical synthesis, $Fe_2(SO_4)_3 \cdot xH_2O$ (0.04 mmol, 97%, Sigma-Aldrich) and Na_2SO_4 (4.8 mmol) was dissolved in 6 mL of DI water. Then, 2 mL of glacial acetic acid was added in the pale yellow solution under continuous stirring, resulting in an orange solution. The mixed solution was transferred into a 25 mL Teflon-lined stainless steel autoclave where a circular Ti foil ~ 1 cm in diameter or a square Ti foil ~ 1 cm in edge length was placed, which was then heated at 180 °C for 24 h. After the autoclave cooled to room temperature, the Ti foil was cleaned with water and ethanol, and then dried in air. The structural optimization of α-Fe_2O_3 nanorod arrays was achieved by chemical etching. A Ti foil with α-Fe_2O_3 nanorod arrays grown on one surface was immersed in a petri dish containing 10 mL of solution containing 1 M of oxalic acid and 100 μM of $FeSO_4$, and placed at 26 °C for a certain time.

Characterization

The products were characterized by scanning electron microscopy (SEM, Hitachi S4800, 5kV), transmission electron microscopy (TEM, FEI Tecnai F30, 300 kV), and X-ray diffraction (XRD, Rigaku Dmax-2000, Cu Kα radiation).

Electrochemical measurements

A circular Ti foil with a diameter of ~ 1 cm was used as the substrate for the growth of α-Fe_2O_3 nanorod arrays, which were calcined at 450 °C for 30 min in air to remove organics and dried under vacuum at 120 °C overnight before electrochemical measurements. The weight of α-Fe_2O_3 was calculated by subtracting the weight of the rare Ti foil from that of the Ti foil with α-Fe_2O_3 nanorod arrays. The Ti foil with α-Fe_2O_3 nanorod arrays grown on one face was directly used as a binder-free anode in 2032 coin cell, which was assembled in an argon-filled glovebox. The bare face of Ti foil was located close to the outside shell of the cell. Li foil was used as the counter electrode, 1 M $LiClO_4$ in propylene carbonate (PC) and dimethyl carbonate (1:1 by volume) was used as the electrolyte, and Celgard 2400 was used as the separator. Flexible full batteries were assembled by using Ti foil with α-Fe_2O_3 nanorod arrays as binder-free anodes, Al foil with commercial $LiFePO_4$ loaded as cathodes, and Celgard 2400 as

separator. The electrodes were cut into squares of 2.7 cm × 4.2 cm with small feet to connect with wires. The electrolyte was dropped on both anode and cathode before the whole battery was compacted and sealed by width tape in an argon-filled glovebox. The electrochemical performances were tested by using a LAND CT2001A battery test system at room temperature (25 °C). The coin cells were charged and discharged between 0.05 V and 3.0 V at a constant current (1 C rate taken to be 1000 mAh g^{-1}), and the flexible full batteries were charged and discharged between 0.5 V and 3.2 V at 5 C. Cyclic voltammetry (CV) study was carried out on a CV autolab (Eco Chemie, PGSTAT302N). Electrochemical impedance spectroscopy (EIS) was measured using coin-type half batteries on an analyzer (Shanghai Chenhua, CHI660D) in the frequency range from 10^{-2} to 10^{5} Hz, which were charged and discharged between 0.05 V and 3.0 V at constant currents, similar to the cycling and rate performance tests. All electrochemical tests were measured by several times using different samples to ensure the credibility of data.

Results and discussion

Dense α-Fe_2O_3 nanorod arrays were directly grown on Ti foil by a hydrothermal process in an aqueous $Fe_2(SO_4)_3$ solution containing HAc and Na_2SO_4. A uniform brick-red thin film of α-Fe_2O_3 was grown on Ti foil after hydrothermal reaction for 24 h (Fig. S1, ESI†). Fig. 2a shows a typical low-magnification SEM image of the as-grown α-Fe_2O_3 nanorod arrays, which suggests the formation of a thin film consisting of densely grown arrays of bundled nanorods. An enlarged image shown in Fig. 2b suggests that the nanorod bundles with rough surfaces have an average diameter of ~150 nm. A typical cross-sectional SEM image suggests that the vertically aligned nanorod arrays have a length of ~350 nm (Fig. 2c). Fig. 2d shows a representative TEM image, which suggests that each bundle consists of primary nanorods ~10 nm in diameter emanating radially from the root. The corresponding selected-area electron diffraction (SAED) pattern exhibits elongated diffraction spots corresponding to the [010] zone axis of hematite, indicating that each nanorod bundle is basically a [001]-oriented α-Fe_2O_3 mesocrystal. The high-resolution TEM (HRTEM) image shown in Fig. 2e exhibits clear lattice fringes with spacings of 0.23 nm and 0.25 nm, which correspond to the (006) and (110) planes of α-Fe_2O_3, respectively, indicating that each primary nanorod is a [001]-oriented α-Fe_2O_3 single crystal. The XRD pattern shown in Fig. 2f suggests the formation of pure hematite crystals (JCPDS No. 33-0664) on the Ti substrate. The decrease in the intensity of the (110) peak compared with the standard pattern is in good agreement with the [001]-directed growth indicated by the SAED and HRTEM results. To the best of our knowledge, it is for the first time that ordered α-Fe_2O_3 nanoarrays consisting of nanorod bundles with a mesocrystalline structure have been directly grown on a solid substrate by hydrothermal growth. It may be noted that the previously reported solution-processed α-Fe_2O_3 nanoarrays were normally polycrystalline α-Fe_2O_3 nanostructures resulting from the conversion from the initial FeOOH nanoarrays by annealing.[21-23] The current mesocrystalline α-Fe_2O_3 nanorod bundles may be beneficial to the formation of robust nanorod arrays on substrate, which are able to accommodate considerable mechanical stresses.

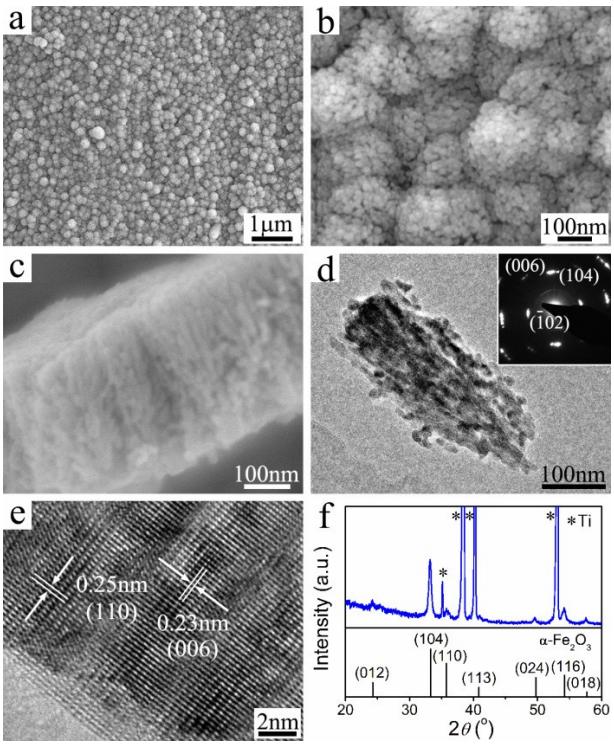

Fig. 2 SEM (a-c), TEM (d), and HRTEM (e) images and XRD pattern (f) of pristine α-Fe_2O_3 nanorod arrays grown on Ti foil. Inset in (d) is the corresponding SAED pattern.

In the hydrothermal reaction system involving HAc and Na_2SO_4, appropriate concentrations of Fe^{3+} ions, HAc, and SO_4^{2-} ions are essential to the formation of the unique robust α-Fe_2O_3 nanorod arrays. Typically, the α-Fe_2O_3 nanoarrays shown in Fig. 2 were obtained at concentrations of 5 mM, 4.2 M, and 0.6 M for $Fe_2(SO_4)_3$, HAc, and Na_2SO_4, respectively. An increase in the reactant concentration would increase the supersaturation, leading to a transition from heterogeneous nucleation on substrate to homogeneous nucleation in solution. For example, sparser arrays of shorter α-Fe_2O_3 nanorods were achieved at a lower $Fe_2(SO_4)_3$ concentration (2.5 mM), whereas dumbbell-like α-Fe_2O_3 microparticles were precipitated when the $Fe_2(SO_4)_3$ concentration was increased to 15 mM (Fig. S2, ESI†). HAc played a key role in controlling the hydrolysis rate of Fe(III) species by coordination of Ac^- ions with Fe(III) and control of pH. At lower HAc concentrations, precipitation of nanoparticles or large aggregates occurred because of higher hydrolysis rates; in contrast, aligned arrays of nanorod bundles ~400 nm in diameter were achieved at a higher HAc concentration (Fig. S3, ESI†). Furthermore, the additive Na_2SO_4 played an important role in controlling the diameter of the primary α-Fe_2O_3 nanorods and the interstices between them through the preferential adsorption of sulfate ions on the surfaces parallel to the [001] direction of hematite. It has been documented that in acidic solutions, the adsorption of sulfate ions on the surface of hematite led to the

[001]-oriented growth of α-Fe_2O_3 nanorods and favored the formation of radial hierarchical structures.[39,40] In the current situation, loose arrays of α-Fe_2O_3 nanorods with diameters as large as ~100 nm were produced without the addition of Na_2SO_4, and the diameter of the primary nanorods and the interstices between them were gradually decreased with increasing Na_2SO_4 concentration (Fig. S4, ESI†).

In order to achieve enough spaces for accommodating the lithiation-induced volume expansion of α-Fe_2O_3 nanorods, a chemical etching method was introduced to realize the structural optimization of the α-Fe_2O_3 nanorod arrays. The controlled $H_2C_2O_4$ etching process has been previously employed for the top-down fabrication of α-Fe_2O_3 single-crystal nanodiscs and microparticles with tunable porosity.[9] In the current etching process, 1 M $H_2C_2O_4$ was employed as the etchant and 100 μM of Fe^{2+} ions were added in advance as the catalyst to keep a constant etching rate. It was found that the interstices between α-Fe_2O_3 nanorods were gradually enlarged with etching time while the diameter and length of the nanorods remained essentially unchanged (Fig. S5, ESI†). It indicated that the less stable nanorods were preferentially etched off. When the etching time was increased up to 1.5 h, the nanorod arrays kept adherence to the substrate and maintained the structural integration. A weight loss about 63% was measured for the α-Fe_2O_3 nanorods on Ti substrate after 1.5 h of etching, which suggests that enough spaces have been created for the volume expand of α-Fe_2O_3 during lithiation (70 ~ 80%).[41] When the etching time was further prolonged to 2 h, most of the nanorod arrays were detached from the substrate, indicating that the roots of the nanorod bundles were broken due to excessive etching. Thus, the α-Fe_2O_3 nanorod arrays after etching for 1.5 h with a stable nanoarray structure and the largest interstices have an optimized structure for self-supported 3D anodes for high-rate LIBs.

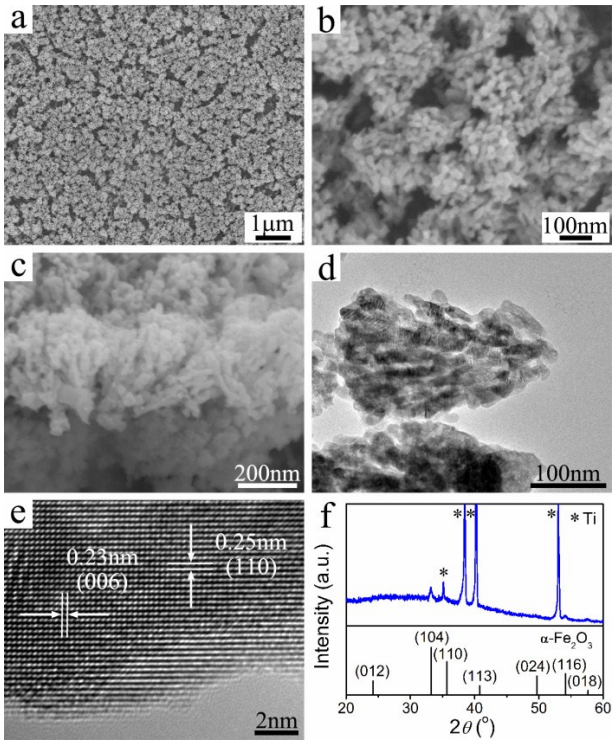

Fig. 3 SEM (a-c), TEM (d), and HRTEM (e) images and XRD pattern (f) of α-Fe_2O_3 nanorod arrays after etching for 1.5 h (Fe_2O_3-NA-1.5).

The α-Fe_2O_3 nanorod arrays after etching were annealed at 450 °C for 30 min in air to remove organics and enhance the adherence to the Ti substrate before electrochemical tests. Fig. 3 shows structural characterizations of the annealed α-Fe_2O_3 nanorod arrays after 1.5 h of etching (Fe_2O_3-NA-1.5). It can be seen that the nanorod arrays with significantly expanded interstices kept their original morphology after annealing (Fig. 3a,b). The cross-sectional observation clearly shows the expanded interstices between nanorods in the inner part of the self-supported nanoarrays (Fig. 3c). The cross-sectional SEM images of the α-Fe_2O_3 nanorod arrays on Ti foil obtained by cutting with scissors suggest that both α-Fe_2O_3 nanorod arrays before and after etching adhered strongly to the Ti substrate while the SEM image of the etched sample after annealing showed a better resolution because of the removal of residual organics (Fig. S6, ESI†). Fig. 3d presents a typical TEM image of a bundle of α-Fe_2O_3 nanorods with a diameter ~ 10 nm, which shows that the width of the interstices between nanorods or the pore size within the nanorod bundle is nearly 10 nm. The HRTEM image shown in Fig. 3e shows lattice fringes with spacings of 0.23 nm and 0.25 nm, which correspond to the (006) and (110) planes of hematite α-Fe_2O_3, respectively. The XRD pattern of the nanorod arrays after etching only shows the (104) and (116) peaks of hematite (Fig. 3f), which is consistent with the considerable mass loss of the α-Fe_2O_3 nanoarrays on Ti substrate upon etching.

The obtained α-Fe_2O_3 nanorod arrays with optimized interstices are attractive for high-rate LIBs since they are favorable for electronic transport and ionic diffusion and allow for volume expansion and strain relaxation (Fig. 1b). Therefore, the optimized α-Fe_2O_3 nanorod arrays on Ti foil (Fe_2O_3-NA-1.5) were directly used as binder-free anodes for LIBs in coin-type half batteries. Fig. 4a shows the initial five cyclic voltammetry (CV) curves of Fe_2O_3-NA-1.5 at a scan rate of 0.5 mV s^{-1} in the potential range from 3.0 to 0.05 V (vs. Li^+/Li). The electro-chemical reaction of α-Fe_2O_3 in LIBs can be described as the conversion reaction mechanism:

$$Fe_2O_3 + 6Li^+ + 6e^- \leftrightarrow 2Fe + 3Li_2O$$

Similar to the previous reports, the minor cathodic peak around 1.6 V corresponds to the initial lithiation of Fe_2O_3 to $Li_xFe_2O_3$, and another well-defined cathodic peak around 0.65 V is caused by the reduction of Fe(III) to Fe and the formation of solid electrolyte interphase (SEI).[14,20] The broad anodic peaks from 1.7 to 2.2 V are associated with the reversible multistep oxidation of Fe to FeO and then to Fe_2O_3.[18] The discharge/charge voltage profiles of Fe_2O_3-NA-1.5 at a current density of 1 C (1 C was taken to be 1000 mAh g^{-1}) from 3.0 to 0.05 V are shown in Fig. 4b. The α-Fe_2O_3 nanorod arrays exhibited initial discharge and charge capacities of 1238 and

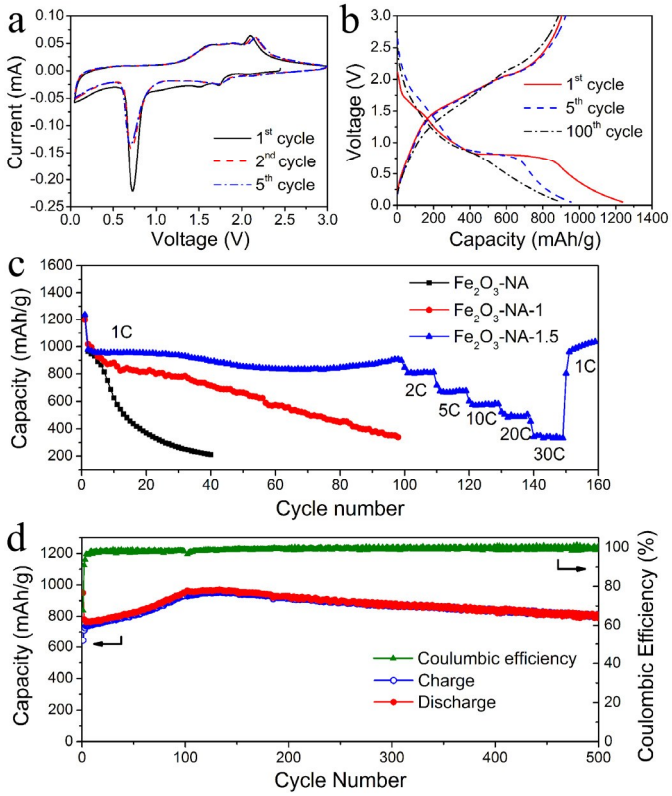

Fig. 4 Electrochemical properties of α-Fe_2O_3 nanorod arrays: Cyclic voltammetry curve at a scan rate of 0.5 mV/s (a) and voltage profiles at 1 C (b) of Fe_2O_3-NA-1.5. (c) Cycling performance at 1 C of α-Fe_2O_3 nanorod arrays with different etching times and rate performance of Fe_2O_3-NA-1.5. (d) Cycling performance and Coulombic efficiency of Fe_2O_3-NA-1.5 at 5 C.

904 mAh g^{-1}, respectively. During the subsequent cycles, the electrode showed good cycling stability and kept a discharge capacity of 955 mAh g^{-1} after 100 cycles, which is very close to the theoretical capacity of α-Fe_2O_3. Taking into account the loading density of α-Fe_2O_3 on Ti substrate (~0.042 mg cm^{-2}), an areal capacity ~40 μAh cm^{-2} was estimated for the self-supported 3D anode after 100 cycles at 1 C. The low loading density seems a common problem associated with nanoarrays grown on planar substrates, which could be further solved by growing longer α-Fe_2O_3 nanorods or using substrates with 3D structures for the growth of larger amounts of nanoarrays. Fig. 4c shows the cycle performance of α-Fe_2O_3 nanorod arrays with different etching times at 1 C together with the rate performance of Fe_2O_3-NA-1.5. Compared with the pristine α-Fe_2O_3 nanorod arrays (Fe_2O_3-NA) and the nanorod arrays after 1 h of etching (Fe_2O_3-NA-1), Fe_2O_3-NA-1.5 exhibited the best cycling performance with a high capacity around 950 mAh g^{-1} within 100 cycles, while the capacity of Fe_2O_3-NA-1 fell to 340 mAh g^{-1} after 100 cycles and the capacity of Fe_2O_3-NA dropped to 210 mAh g^{-1} after only 40 cycles. The Nyquist plots of Fe_2O_3-NA and Fe_2O_3-NA-1.5 before cycling show semicircles from the high to the medium frequency region that can be attributed to the combination of contact resistance between the current collector and active material and the charge transfer impedance (Fig. 5a). It is indicated that the etching process

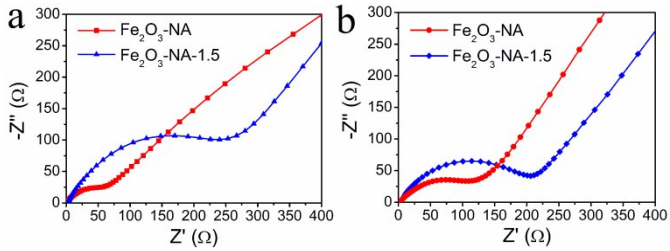

Fig. 5 Nyquist plots of α-Fe_2O_3 nanorod arrays without etching (Fe_2O_3-NA) and after 1.5 h of etching (Fe_2O_3-NA-1.5) before (a) and after (b) 100 cycles.

basically impaired the electron transport from α-Fe_2O_3 nanorod arrays to Ti substrate owing to the decrease in the contact area; nevertheless, the cycling stability was significantly increased despite such an increase in the impedance. Fig. 5b shows the Nyquist plots of Fe_2O_3-NA and Fe_2O_3-NA-1.5 after 100 cycles, which suggest that the impedance of Fe_2O_3-NA almost doubled after cycling, whereas the impedance of Fe_2O_3-NA-1.5 did not show considerable change. Therefore, the pronounced improvement of cycling stability upon etching could be mainly attributed to the expanded interstices providing enough space to mitigate the volume variations associated with lithium storage, resulting in a stable structure during cycling.

It is noteworthy that Fe_2O_3-NA-1.5 exhibited excellent rate capability with high reversible capacities of 499 and 350 mAh g^{-1} at high discharge/charge rates of 20 and 30 C (Fig. 4c), which is of great importance for designing future fast-charging LIBs. For example, at a high rate of 30 C (30 A g^{-1}), the Fe_2O_3-NA-1.5 anode can be fully charged or discharged within 2 minutes with an acceptable capacity of 350 mAh g^{-1}, which is close to the theoretical capacity of commercially used graphite anode, indicating its potential application in future high-rate batteries. This rate capability is considerably higher than those reported for the α-Fe_2O_3 nanowall arrays (440 mAh g^{-1} at 5 C),[23] mesoporous nanoparticles (424 mAh g^{-1} at 10 C),[10] free-standing nanomembranes (354 mAh g^{-1} at 20 C),[20] as well as the composite materials of α-Fe_2O_3 with graphene (370 mAh g^{-1} at 6 A g^{-1})[24] and CNTs (420 mAh g^{-1} at 3 A g^{-1}).[26] The superior rate performance of the α-Fe_2O_3 nanorod arrays can be ascribed to the efficient electrical and ionic transport provided by the robust nanorod arrays grown directly on conductive substrate. To further explore the electrode performance of high-rate LIBs, the cycling performance of Fe_2O_3-NA-1.5 at a high rate of 5 C was tested, which is shown in Fig. 4d. The α-Fe_2O_3 nanorod arrays achieved a reversible capacity of 782 mAh g^{-1} at first, and a highest capacity of 970 mAh g^{-1} at the 130th cycle. The capacity increase in the first 130 cycles could be ascribed to the reversible lithium storage in the polymeric gel-type layer which built up slowly at the first hundred cycles.[14] In the subsequent cycles, the capacity was decreased slowly, and retained a high capacity of 801 mAh g^{-1} after 500 cycles. The SEM images of Fe_2O_3-NA-1.5 after 500 cycles at 5 C show that the initial nanoarray structure was essentially preserved (Fig. S7a,b, ESI†). A typical cross-sectional SEM image of Fe_2O_3-NA-1.5 after 100 cycles suggests that the nanoarrays still strongly adhered to the Ti substrate (Fig. S7c,

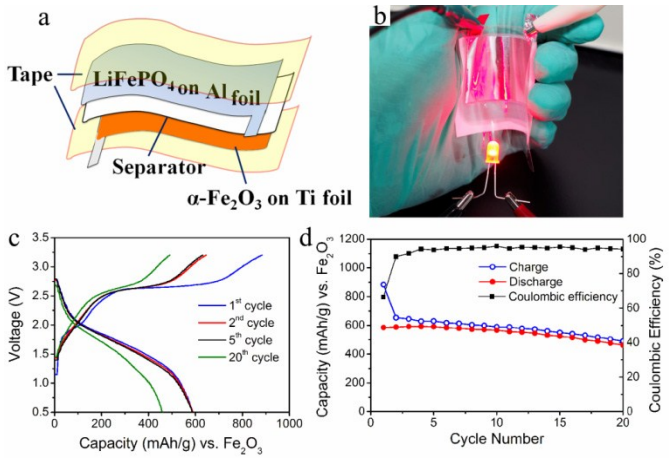

Fig. 6 (a) Schematic illustration of a flexible lithium ion battery assembled using Fe_2O_3-NA-1.5 on Ti foil as the anode. (b) Optical photograph of an LED lightened by the bended battery. Voltage profiles (c) and cycling performance (d) of the flexible battery at 5 C.

ESI†). Such an excellent cycling performance at high rate further demonstrates the advantages of the robust nanorod arrays with optimized interstices as self-supported 3D anodes for high-rate LIBs, which might be applicable in high power energy storage devices.

The high performance of the α-Fe_2O_3 nanorod arrays grown on Ti foil as additive-free anodes for high-rate LIBs endows them with great potential for applications in fast-charging flexible batteries.[3,34,42,43] As a preliminary demonstration, a flexible full battery was assembled using Fe_2O_3-NA-1.5 grown on Ti foil with a thickness of ~0.05 mm as the anode and commercial $LiFePO_4$ loaded on Al foil as the cathode, as shown in Fig. 6a. The final packaged flexible battery had a thickness of ~0.17 mm, which makes it very soft and easy of bending (Fig. S8, ESI†). This flexible battery was able to light a red LED whether it was flat or bended, as shown in Fig. 6b. The voltage profiles and cycling performance of the flexible full battery at a charge/discharge rate of 5 C (1 C = 1000 mA g^{-1}, the current density and specific capacity were calculated by the mass of Fe_2O_3) from 0.5 to 3.2 V, were presented in Fig. 6c and d, respectively. The α-Fe_2O_3 nanoarray electrode exhibited initial charge and discharge capacities of 884 and 586 mAh g^{-1} in a full battery, respectively, and retained a stable reversible capacity within 20 cycles. The specific capacity and cyclability of the nanoarray electrode in flexible full batteries were somewhat lower than those in coin-type half batteries, which might be attributed to the increased internal resistance and the sealing deficiency of the primary flexible full battery. Furthermore, a preliminary test of the cycling performance of the flexible battery at varied bending states at 5 C suggests that a significant bending of the battery did not bring about a considerable change in the cycling performance despite a relatively faster capacity fading upon bending possibly owing to the sealing deficiency (Fig. S9, ESI†). The fast-charging capability, high specific capacity, and bendable properties of the α-Fe_2O_3 nanoarray anodes make them potentially applicable in roll-up displays, portable bendable electronics, and wearable devices.

Conclusions

In conclusion, we have developed a facile method to achieve robust α-Fe_2O_3 nanorod arrays on Ti substrate with tunable interstices through a sulfate ion-assisted hydrothermal reaction in HAc solution followed by chemical etching. The mesocrystalline α-Fe_2O_3 nanorod arrays with optimized interstices are favorable for ionic diffusion and allow for volume expansion and strain relaxation, and the self-supported nanorod arrays directly grown on conductive substrate provide effective electron transport pathways, leading to novel 3D anodes with significantly improved rate capability and cyclability. The optimized α-Fe_2O_3 nanorod arrays exhibited excellent cyclability (retained a reversible capacity of 801 mAh g^{-1} after 500 cycles at a discharge/charge rate of 5 C) and high rate capability (499 mAh g^{-1} at 20 C and 350 mAh g^{-1} at 30 C) when used as a binder-free anode for LIBs. Moreover, a flexible LIB full battery with a high anode capacity was assembled by using the α-Fe_2O_3 nanorod arrays as the anode. The high performance of the α-Fe_2O_3 nanorod arrays as novel 3D anodes for high-rate LIBs indicates their practical applications in fast-charging batteries for microscale energy storage devices and flexible electronics. Considering the characteristics of high abundance and non-toxicity for α-Fe_2O_3 and the eco-efficient synthetic process, this approach may open new pathways towards greener and more sustainable batteries for electric energy storage.[7] Furthermore, the synthetic strategy based on solution-phase growth coupled with chemical etching could be extended to other metal oxide systems, thus providing an effective solution to the problems associated with rate capability and cyclability.

Acknowledgements

This work was supported by NSFC (Grant Nos. 21173010 and 21473004) and MOST (Grant No. 2013CB932601).

Notes and references

1 M. Armand and J. M. Tarascon, *Nature*, 2008, **451**, 652.
2 Z. Wang, L. Zhou and X. W. Lou, *Adv. Mater.*, 2012, **24**, 1903.
3 G. Zhou, F. Li and H.-M. Cheng, *Energy Environ. Sci.*, 2014, **7**, 1307.
4 J. Jiang, Y. Li , J. Liu, X. Huang, C. Yuan and X. W. Lou, *Adv. Mater.*, 2012, **24**, 5166.
5 Q. Zhang, E. Uchaker, S. L. Candelaria and G. Cao, *Chem. Soc. Rev.*, 2013, **42**, 3127.
6 M. V. Reddy, G. V. Subba Rao and B. V. R. Chowdari, *Chem. Rev.*, 2013, **113**, 5364.
7 D. Larcher and J. M. Tarascon, *Nat. Chem.*, 2015, **7**, 19.
8 L. Zhang, H. B. Wu, X. W. Lou, *Adv. Energy Mater.*, 2014, **4**, 1300958.
9 J. S. Chen, T. Zhu, X. H. Yang, H. G. Yang and X. W. Lou, *J. Am. Chem. Soc.* 2010, **132**, 13162.
10 X. Xu, R. Cao, S. Jeong and J. Cho, *Nano Lett.*, 2012, **12**, 4988.
11 B. Wang, J. S. Chen, H. B. Wu, Z. Y. Wang and X. W. Lou, *J. Am. Chem. Soc.*, 2011, **133**, 17146.
12 L. Zhang, H. B. Wu, S. Madhavi, H. H. Hng and X. W. Lou, *J. Am. Chem. Soc.*, 2012, **134**, 17388.

13 L. Zhang, H. B. Wu and X. W. Lou, *J. Am. Chem. Soc.*, 2013, **135**, 10664.
14 J. Zhu, Z. Yin, D. Yang, T. Sun, H. Yu, H. E. Hoster, H. H. Hng, H. Zhang and Q. Yan, *Energy Environ. Sci.*, 2013, **6**, 987.
15 J. Miot, N. Recham, D. Larcher, F. Guyot, J. Brest and J. M. Tarascon, *Energy Environ. Sci.* 2014, **7**, 451.
16 S. Xu, C. M. Hessel, H. Ren, R. Yu, Q. Jin, M. Yang, H. Zhao and D. Wang, *Energy Environ. Sci.*, 2014, **7**, 632.
17 Z. An, J. Zhang, S. Pan, F. Yu, *J. Phys. Chem. C*, 2009, **113**, 8092.
18 X. Duan, L. Mei, J. Ma, Q. Li, T. Wang, W. Zheng, *Chem. Commun.*, 2012, **48**, 12204.
19 Z. Wang, D. Luan, S. Madhavi, C. M. Li and X. W. Lou, *Chem. Commun.*, 2011, **47**, 8061.
20 X. Liu, W. Si, J. Zhang, X. Sun, J. Deng, S. Baunack, S. Oswald, L. Liu, C. Yan and O. G. Schmidt, *Sci. Rep.*, 2014, **4**, 7452.
21 Y. Song, S. Qin, Y. Zhang, W. Gao and J. Liu, *J. Phys. Chem. C*, 2010, **114**, 21158.
22 J. Liu, Y. Li, H. Fan, Z. Zhu, J. Jiang, R. Ding, Y. Hu and X. Huang, *Chem. Mater.*, 2010, **22**, 212.
23 D. Lei, M. Zhang, B. Qu, L. Chen, Y. Wang, E. Zhang, Z. Xu, Q. Li and T. Wang, *Nanoscale*, 2012, **4**, 3422.
24 R. Wang, C. Xu, M. Du, J. Sun, L. Gao, P. Zhang, H. Yao and C. Lin, *Small*, 2014, **10**, 2260.
25 Y. Yang, X. Fan, G. Casillas, Z. Peng, G. Ruan, G. Wang, M. J. Yacaman, J. M. Tour, *ACS Nano*, 2014, **8**, 3939.
26 Z. Wang, D. Luan, S. Madhavi, Y. Hu and X. W. Lou, *Energy Environ. Sci.*, 2012, **5**, 5252.
27 J.-M. Jeong, B. G. Choi, S. C. Lee, K. G. Lee, S.-J. Chang, Y.-K. Han, Y. B. Lee, H. U. Lee, S. Kwon, G. Lee, C.-S. Lee and Y. S. Huh, *Adv. Mater.*, 2013, **25**, 6250.
28 J. Liu, W. Zhou, L. Lai, H. Yang, S. Hua Lim, Y. Zhen, T. Yu, Z. Shen and J. Lin, *Nano Energy*, 2013, **2**, 726.
29 B. L. Ellis, P. Knauth and T. Djenizian, *Adv. Mater.*, 2014, **26**, 3368.
30 J.-Y. Liao, D. Higgins, G. Lui, V. Chabot, X. Xiao and Z. Chen, *Nano Lett.*, 2013, **13**, 5467.
31 Y. Yang, Z. Peng, G. Wang, G. Ruan, X. Fan, L. Li, H. Fei, R. H. Hauge, J. M. Tour, *ACS Nano*, 2014, **8**, 7279.
32 J.-Y. Liao and A. Manthiram, *Adv. Energy Mater.*, 2014, **4**, 1400403.
33 S. Chen, M. Wang, J. Ye, J. Cai, Y. Ma, H. Zhou and L. Qi, *Nano Res.*, 2013, **6**, 243.
34 S. Chen, Y. Xin, Y. Zhou, Y. Ma, H. Zhou and L. Qi, *Energy Environ. Sci.*, 2014, **7**, 1924.
35 X. Wang, X. Lu, B. Liu, D. Chen, Y. Tong and G. Shen, *Adv. Mater.*, 2014, **26**, 4763.
36 R.-Q. Song and H. Cölfen, *Adv. Mater.*, 2010, **22**, 1301.
37 J. Ye, W. Liu, J. Cai, S. Chen, X. Zhao, H, Zhou, L. Qi, *J. Am. Chem. Soc.*, 2011, **133**, 933.
38 E. Uchaker and G. Cao, *Nano Today*, 2014, **9**, 499.
39 T. Sugimoto and Y. Wang, *J. Colloid Interface Sci.*, 1998, **207**, 137.
40 N. Sasaki, Y. Murakami, D. Shindo and T. Sugimoto, *J. Colloid Interface Sci.*, 1999, **213**, 121.
41 Q. Su, D. Xie, J. Zhang, G. Du, B. Xu, *ACS Nano*, 2013, **7**, 9115.
42 B. Liu, J. Zhang, X. Wang, G. Chen, D. Chen, C. Zhou, G. Shen, *Nano Lett.*, 2012, **12**, 3005.
43 M.-H. Park, M. Noh, S. Lee, M. Ko, S. Chae, S. Sim, S. Choi, H. Kim, H. Nam, S. Park and J. Cho, *Nano Lett.*, 2014, **14**, 4083.

Graphical abstract for contents entry

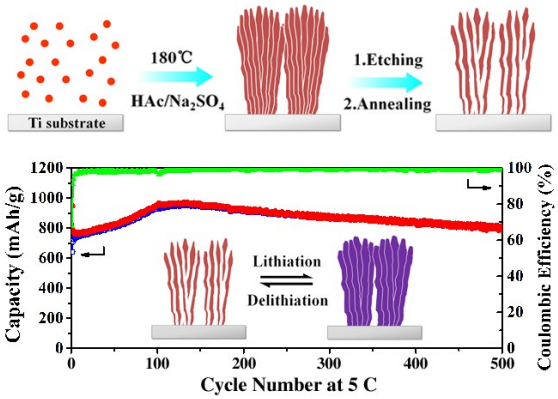

Robust α-Fe_2O_3 nanorod arrays with optimized interstices are used as self-supported 3D anodes with significantly improved rate capability and cyclability.